Origin of Light-Harvesting Enhancement in Colloidal-Photonic-Crystal-Based Dye-Sensitized Solar Cells

A. Mihi and H. Míguez*

Instituto de Ciencia de Materiales de Sevilla, Consejo Superior de Investigaciones Científicas, Avda. Américo Vespucio s/n, Isla de la Cartuja, 41092 Sevilla, Spain

Received: April 8, 2005

The effect of the presence of a photonic crystal on the optical absorption of dye-sensitized titanium oxide solar cells is theoretically investigated herein. Different configurations in which a colloidal crystal can be implemented in such devices are modeled, and their absorptances compared. Experimental results on light-harvesting enhancement recently reported for periodically structured photoelectrodes are satisfactorily explained in terms of the appearance of multiple resonant modes localized in the absorbing layer when this is deposited onto one of the optical lattice surfaces. Longer matter−radiation interaction times for such frequencies result in higher absorption of those modes when compared to standard dye-sensitized solar cells. The effect of the finite size and the different characteristics of the photonic crystal on the optical absorption amplification effect is also discussed, new perspectives for colloidal-crystal-based photovoltaics being proposed.

Introduction

Dye-sensitized solar cells (DSSCs) are a promising alternative to conventional photovoltaic devices based on p−n junctions.[1,2] DSSCs combine a solid wide-band-gap semiconductor with a liquid ionic conductor. They consist of one electrode made of a thin layer (typically around 10 μm) of titanium dioxide nanocrystals (nc-TiO_2, about 10 nm in size), on whose surface a dye, typically a ruthenium polypyridyl complex, is adsorbed. This nanocrystalline film is deposited onto a conductive, transparent substrate, typically indium tin oxide (ITO) or SnO_2, and soaked in a redox electrolyte, typically containing I^-/I_3^-, which is in turn in contact with a platinum counter electrode. Sun light is harvested by the dye from which the photoexcited electrons are injected into the bulk of the nanocrystalline semiconductor network and then into the conducting substrate. At the same time, the redox electrolyte reduces the oxidized dye and transports the positive charges to the counter electrode.[3]

Since they are made of inexpensive materials that are processed at low temperatures, these devices have attracted a great deal of attention over the past few decades in the field of alternative energy resources. However, from a fundamental point of view, their main drawback when compared to their silicon p−n junction relatives is their lower light-to-electric power conversion efficiency. A great effort has been made to improve it, but the over 10% efficiencies currently achieved[4] still remain far below that of their silicon counterparts.[5] In this sense, diverse strategies have been followed to enhance the performance of DSSCs, targeting the increase in the output voltage or the photogenerated current, alternatively. Metal oxides having a more negative conduction band potential have been used as photoelectrodes to improve the former,[6−8] while dyes having a wider absorption band[9] or higher molar extinction coefficients[10] have been tested as sensitizers to enhance the latter.

Particularly relevant prior work to that presented herein are those studies whose target is the improvement of the photogenerated current by changing the optical design of the cell to optimize its light-harvesting efficiency (LHE), thus making a more efficient use of the solar spectrum.[11] The LHE at a certain wavelength is defined as the fraction of incident photons that are absorbed by the dye, i.e., the absorptance $A = I_A/I_0$, where I_0 is the incident intensity and I_A is the absorbed fraction. The relation between the LHE or absorptance (A) of a solar cell and the photogenerated current density J_{SC} is given by the expression[12]

$$J_{SC} = \int q\Phi(\lambda)\xi(\lambda)\mathrm{LHE}(\lambda)F(\lambda)\,\mathrm{d}\lambda \qquad (1)$$

where q is the electron charge, $\Phi(\lambda)$ is the electron-transfer yield, $\xi(\lambda)$ is a factor that accounts for the losses at the air−substrate interface, and $F(\lambda)$ is the ratio between the solar spectral irradiance and the photon energy.

Under this scope, larger LHE, and therefore larger J_{SC}, at the long-wavelength side of the dye absorption band have been demonstrated by inserting a film made of strongly scattering particles either below[13] or within[12] the dye-sensitized nc-TiO_2 layer. Different designs have been tested to optimize the optical response of the cell based on this concept,[14−17] most of them using disordered, polydisperse packings of submicron-sized spheres as highly diffusive reflecting layers.

Very recently, by structuring the absorbing active layer in the shape of a photonic crystal,[18] Mallouk et al. achieved a 26% enhancement of the photogenerated current with respect to a conventional (i.e., nonperiodically structured) photoelectrode.[19] The novelty of this approach with respect to previous ones lies in the fact that the strongly scattering dye-sensitized photoelectrode is made of highly scattering centers periodically arranged in a three-dimensional lattice, i.e., a photonic crystal structure coupled to a conventional nc-TiO_2 film. The originality of the proposal and the large increase in efficiency reported have generated a considerable deal of interest.[20,21] Such enhancement was originally attributed to the amplification of optical absorp-

* Author to whom correspondence should be addressed. E-mail: hernan@icmse.csic.es.

10.1021/jp051828g CCC: $30.25
Published on Web 07/30/2005

tion resulting from the anomalous propagation of light through the photonic crystal part of the cell. On the basis of previous theoretical and experimental work,[22] Mallouk et al. proposed that the absorption enhancement could in principle be caused by the slow speed of photons as well as their preferential flight through the absorbing material path when travelling along the photonic crystal. These phenomena should take place at frequencies for which the dispersion relation is very flat, which occurs for a narrow range of energies below the characteristic stop band of these photonic crystals.[23,24] However, some aspects of the observed enhancement remained unclear or were apparently contradictory, as exposed in what follows. First, the enhancement reported in ref 19 takes place for a frequency range that is at least 10 times larger than the expected one.[25] Second, it is observed for modes that do not propagate through the photonic crystal, since their energy matches the forbidden band of the crystal. Finally, the enhancement is only observed when the cell is illuminated from the usually considered rear side, that is, the counter electrode side, while a decrease in efficiency is attained when illuminated from the front side. Further recent work by the same authors focused on the experimental analysis of the optical response of the different parts of the reported cell considered both separately and combined.[26] After this deeper insight into the question of the origin of LHE enhancement, Mallouk et al. concluded that the observed increase in efficiency was the result of two different effects of different magnitudes: on one side, and less important, the enhancement of red absorbance due to slow photon propagation in the dye-sensitized inverse opal; on the other, and most importantly, the localization of light within the conventional dye-sensitized nc-TiO_2 slab as a result of the incoherent scattering caused by disordered regions of the photonic crystal.

In this paper, we seek to shed light on the origin of the enhancement of light-harvesting efficiency observed when a photonic crystal is introduced into nc-TiO_2 DSSCs. We have theoretically analyzed the optical absorption properties of different realistic configurations, paying particular attention to that previously reported in ref 19. An alternative explanation to all of the LHE enhancement effects is provided, which are accounted for without considering the presence of disorder or defects in the photonic crystal. We found out that significant optical absorption amplification over a wide spectral range occurs only in structures that combine the presence of a photonic crystal and a thin layer of nonperiodically structured absorbing material. Our analysis indicates that this effect is mainly the consequence of partial localization of light within the latter, rather than in the former, contrary to what had originally been proposed[19] and in good agreement with a recently proposed hypothesis.[26] However, light localization is the result of the appearance of multiple resonant modes resulting from the presence of an interface between a photonic crystal and an absorbing slab on one of the lattice surfaces.[27] Both the spectral response and the asymmetric behavior (rear versus front side illumination) reported are successfully explained in these terms, without considering any contribution of incoherent scattering from possible disordered regions of the photonic crystal. The expected increase in photocurrent efficiency is also quantified, a fair agreement with the reported data being found. Interestingly, our calculations show that there is no need to structure the light-harvesting material in the shape of a photonic crystal, efficient absorption being attained for a DSSC in which an absorbing slab and a nonabsorbing and highly reflecting photonic crystal are coupled.

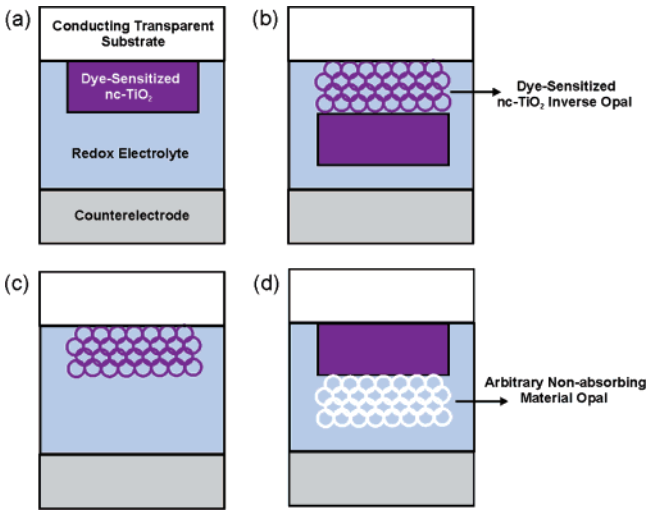

Figure 1. Schemes of the DSSCs whose LHEs are herein analyzed. (a) A standard DSSC made of a dye-sensitized nc-TiO_2 film grown onto a conductive glass substrate. (b) A photonic-crystal-based DSSC in which a dye-sensitized nc-TiO_2 film is grown onto a dye-sensitized nc-TiO_2 inverse opal, which is in turn deposited on a conductive glass. (c) Dye-sensitized nc-TiO_2 inverse opal deposited on a conductive glass. (d) Nonabsorbing photonic crystal (arbitrary material) built onto a dye-sensitized nc-TiO_2 film, which is in turn deposited on the surface of a conductive glass. In all cases, the photoelectrode is embedded in electrolyte.

Results and Discussion

Structure of the Photonic-Crystal-Based Dye-Sensitized Solar Cell. To start our analysis of the optical properties of photonic-crystal-based DSSCs, we carefully considered the structure and the values of all relevant parameters of the system for which increased light-harvesting efficiency was recently reported. In ref 19, a three-dimensional face-centered cubic (fcc) lattice of interconnected spherical cavities whose walls were made of dye-sensitized nc-TiO_2, which we will refer to as *inverse opal* hereinafter, was built onto a fluorinated tin oxide transparent conducting substrate. A combination of colloidal crystallization and liquid-phase deposition techniques was used to achieve this goal. By doing so, a stacking of close-packed spherical cavity planes parallel to the substrate is achieved, hence the [111] direction of the fcc crystal being perpendicular to the conducting substrate. Also, a layer of commercially available dye-sensitized nc-TiO_2 was deposited onto the inverse opal by squeegee-printing, and after the cell was sealed, all of the interstitial space was infiltrated with redox electrolyte. The final structure of the resulting photoelectrode described in ref 19 is depicted in Figure 1b as well as those of a standard DSSC and other photonic-crystal-based cells whose properties are also analyzed herein for the sake of comparison.

Theoretical Approach: The Scalar Wave Approximation. A distinct feature of photonic crystals is their ability to diffract light, which in the case of titania inverse opals results in a characteristic strong, colored reflection.[28,29] Light modes within such periodic dielectrics can be described in terms of photon energy bands, analogous to electrons in semiconductors.[18] In this framework, the reflectance peaks responsible for the observed color are the consequence of the absence of photon states (stop bands or gaps) along the particular crystalline direction under analysis. Both the band structure and the optical response of the inverse titania opal under study were calculated using a scalar wave approximation (SWA). Although full details on SWA can be found in the literature,[30−32] let us overview the assumptions we made when using this method.

First, the polarization of light (i.e., its vector nature) is neglected. The wave equation for the electric field is then

$$-\nabla^2 E(\vec{\mathbf{r}}) - \frac{\omega^2}{c^2}\epsilon(\vec{\mathbf{r}})E(\vec{\mathbf{r}}) = \frac{\omega^2}{c^2}\epsilon_0 E(\vec{\mathbf{r}}) \tag{2}$$

where c is the speed of light in a vacuum, ω is photon frequency, ϵ_0 is the volume-averaged dielectric constant of the crystal, and $\epsilon(\vec{\mathbf{r}})$ is its periodically modulated part. ϵ_0 is given by the expression

$$\epsilon_0 = \sum_i \epsilon_i \mathrm{ff}_i \tag{3}$$

where ff_i and ϵ_i are the filling fraction and the dielectric constant of the ith component of the lattice. As for electrons in periodic potentials, we can expand the electric field wave function into a Fourier series

$$E(\vec{\mathbf{r}}) = \sum_k C_{\boldsymbol{k}}\, \mathrm{e}^{i\vec{\mathbf{k}}\vec{\mathbf{r}}} \tag{4}$$

where the wavevector $\vec{\mathbf{k}}$ lies within the first Brillouin zone. The periodic dielectric function is also expanded in a Fourier series, in which the sum is performed over all reciprocal lattice vectors $\mathbf{G}$

$$\epsilon(\vec{\mathbf{r}}) = \sum_G U_G\, \mathrm{e}^{i\vec{\mathbf{G}}\vec{\mathbf{r}}} \tag{5}$$

where U_G are the Fourier coefficients with $U_0 = 0$. For spherical scatterers of radius R, dielectric constant ϵ_s, and filling fraction ff in a medium of dielectric constant ϵ_m[30,33]

$$U_G(\vec{\mathbf{G}} \neq 0) = \frac{3\mathrm{ff}}{(GR)}(\epsilon_s - \epsilon_m)[\sin(GR) - GR\cos(GR)] \tag{6}$$

Substitution of eqs 4 and 5 into eq 2 yields

$$\sum_k k^2 C_k\, \mathrm{e}^{ikx} - \frac{\omega^2}{c^2}\sum_G \sum_k C_k U_G\, \mathrm{e}^{i(k+G)x} = \frac{\omega^2}{c^2}\epsilon_0 \sum_k C_k\, \mathrm{e}^{ikx} \tag{7}$$

Since the factors multiplying a certain Fourier component at both sides of the equation must be equal, we attain the following equation for the coefficients C_k

$$\left(k^2 - \frac{\omega^2}{c^2}\epsilon_0\right)C_k - \frac{\omega^2}{c^2}\sum_G C_{k-G}U_G = 0 \tag{8}$$

in which the coupling of the different field modes through the Fourier components of $\epsilon(\vec{\mathbf{r}})$, U_G, is explicit.

A second assumption is made to simplify eq 8. It is based on the fact that we are interested in the optical properties when light impinges in a specific crystalline direction, that is, the direction perpendicular to the periodic stacking of close-packed spherical cavity planes (namely, the [111] direction in real space or $\Gamma-L$ in the reciprocal one). More specifically, we are only concerned about the optical properties at frequencies close to the first Brillouin zone boundary in that direction (i.e., the L-point). Hence, we can further simplify our problem by shortening the expansion of $\epsilon(\vec{\mathbf{r}})$ using just the Fourier components whose scattering dominates around that point. We will consider that $\epsilon(\vec{\mathbf{r}})$ contains only one Fourier component $U_{G_L} = U_{-G_L}$, where $G_L = 2\pi/d_{[111]}$, $d_{[111]}$ being the interplanar distance in the [111] direction. Also, in the expansion of $E(\vec{\mathbf{r}})$, which will now be function of just one spatial variable, we just consider the contribution of a mode corresponding to k and $k = k - G_L$

$$E(x) = C_k\, \mathrm{e}^{ikx} + C_{k-G_L}\mathrm{e}^{i(k-G_L)x} \tag{9}$$

This approach is valid for $k \approx G_L/2$ as long as $\epsilon_0 \gg U_{G_L}$; that is, the fluctuation of the dielectric constant along $\Gamma-L$ is much smaller than its average value.

The coefficients C_k and C_{k-G_L} can be obtained from the system of homogeneous equations (eq 8), now reduced to just a set of two equations. These have nontrivial solutions provided that the following determinant equation is fulfilled

$$\begin{vmatrix} \left((k-G_L)^2 - \frac{\omega^2}{c^2}\epsilon_0\right) & -\frac{\omega^2}{c^2}U_{-G_L} \\ -\frac{\omega^2}{c^2}U_{G_L} & k^2 - \frac{\omega^2}{c^2}\epsilon_0 \end{vmatrix} = 0 \tag{10}$$

By imposing this, we obtain the dispersion relation around the L-point, that is, the relation between the wave vectors inside the lattice, which we will refer to as k_C from now on, and the frequency of the radiation ω

$$k_C(\omega) = \frac{G_L}{2} \pm F(\omega)$$

$$F(\omega) = \sqrt{\frac{{G_L}^2}{4} + \epsilon_0\frac{\omega^2}{c^2} - \sqrt{{G_L}^2\epsilon_0\frac{\omega^2}{c^2} + {U_{G_L}}^2\frac{\omega^4}{c^4}}} \tag{11}$$

Substituting this result in the homogeneous set of equations (eq 6) provides us with the relation between coefficients of the field within the lattice

$$\eta = \frac{{k_C}^2 - \epsilon_0\frac{\omega^2}{c^2}}{U_G\frac{\omega^2}{c^2}} \tag{12}$$

Thus, we have transformed a three-dimensional vector problem into a one-dimensional scalar one. In fact, the approximation expressed in eq 9 is equivalent to the nearly free-electron assumption usually made to find an approximate solution near a zone boundary in the electron band problem.[34] This simplification has been repeatedly found to provide a fairly good description of experimental results for frequencies corresponding to the lower-energy band region of photonic crystals,[35−37,25] which is the energy range whose optical properties we are dealing with. In the higher-energy band range, however, a full vector wave analysis of the bands is needed.[38]

Absorptance of Slabs Coupled to Finite-Size Photonic Crystals. It is clear from eq 1 that to estimate the changes in the photocurrent generation efficiency of the cells depicted in Figure 1 we need to calculate their absorptance. To do so, calculation of the reflection and transmission coefficients of the fields in the incident and outgoing media is required. The finite sizes of the photonic lattice and of any other slab present, which introduce partially transmitted and reflected waves at each interface, should be taken into account. The following set of equations defining the electric field in each medium needs to be solved

$$E(x) = \begin{cases} \text{incident medium} \Rightarrow e^{ik_i x} + r\, e^{-ik_i x} & (13.1) \\ \text{slab} \Rightarrow C_1\, e^{ik_s x} + C_2\, e^{-ik_s x} & (13.2) \\ \text{crystal} \Rightarrow C_3(e^{ik_c x} + \eta\, e^{i(k_c - G_L)x}) + C_4(e^{-ik_c x} + \eta\, e^{-i(k_c - G_L)x}) & (13.3) \\ \text{outgoing medium} \Rightarrow t\, e^{ik_t x} & (13.4) \end{cases}$$

The crystal modes in eq 13.3 are assumed to be those given by eqs 11 and 12, while k_i, k_s, and k_t are the wavevectors in the homogeneous incident, slab, and outgoing media (refractive indexes n_i, n_s, and n_t, respectively). The frequency-dependent coefficients r, t, and C_i involved are determined by imposing the continuity of the electric field and its derivative between media. The SWA permits easy implementation of frequency-dependent and imaginary refractive indexes, which is relevant to our case. Reflectance (R) and transmittance (T) are determined by calculating the coefficients r and t and using the relations

$$R = |r|^2 \tag{14}$$

$$T = |t|^2 \tag{15}$$

Absorptance (A) spectra are then obtained by employing the equation

$$R + T + A = 1 \tag{16}$$

The group velocity of photons crossing the whole structure may also be estimated from the imaginary part of the transmission coefficient.[25,39] After the whole cell is crossed, the phase shift accumulated by the transmitted wave can be estimated from the argument of the complex transmission coefficient t in eq 13.4

$$t = |t|\, e^{i\Delta\phi(\omega)} \tag{17}$$

$$\Delta\phi = L(k_{\text{eff}}(\omega) - k_t) \tag{18}$$

where L is the total length of the photonic crystal−slab structure and $k_{\text{eff}}(\omega)$ is an effective wave vector in which all of the information on the phase shift introduced by such structure is contained. Since the derivative of the phase with respect to the angular frequency results in the group delay, which is in turn inversely proportional to the effective group velocity $v_g(\omega) = \partial\omega/\partial k_{\text{eff}}$

$$\frac{\partial\Delta\phi(\omega)}{\partial\omega} = L\left(\frac{\partial k_{\text{eff}}(\omega)}{\partial\omega} - \frac{\partial k_t}{\partial\omega}\right) = L\left(\frac{1}{v_g(\omega)} - \frac{n_t}{c}\right) \tag{19}$$

Scalar equations such as those shown in eq 13 have been successfully used to fit optical experimental data of complex planar structures containing photonic crystals, such as colloidal crystal supperlattices,[40] or to describe the effect of slabs both in the bulk[41] or on the surface of photonic crystals.[27] In our case, we will use them to simulate the optical absorption response of the different photonic-crystal-based photovoltaic cells shown in Figure 1.

Absorptance of a Dye-Sensitized nc-TiO_2 Inverse Opal Thin Film. First of all, let us simulate the optical properties of the photonic crystal part of the cell separately. So, we analyze what would be the optical response of a DSSC having just a periodically structured photoelectrode, as in the scheme drawn in Figure 1c. Figure 2a displays the calculated photonic band structure along the [111] direction for energies around the stop band using eq 11. Also, the simulated reflectance and absorptance spectra at normal incidence with respect to that same surface are shown in Figures 2b and 2c, respectively, as well as the group velocity in Figure 2d. For these calculations, we have made use of eqs 14−19, and the values of the relevant parameters were extracted from refs 19 and 29. An excellent agreement was found with the stop-band position reported for the structure showing the increased light-harvesting efficiency in ref 19. We used a cavity diameter of 220 nm (versus the 214 nm reported), a background (the electrolyte, an iodide solution in tetraethylene glycol dimethyl ether) of refractive index $n_m = 1.433$, a photonic crystal thickness of 3 μm, and a real part of the refractive index and a filling fraction of the nc-TiO_2 in the inverse opal of $n_{TiO_2} = 2.25$ and $ff_{TiO_2} = 26\%$, respectively. The validity of the SWA in our particular case was confirmed by introducing these parameters into eqs 3 and 6, from which we obtain $\epsilon_0 = 2.98$ and $|U_{G_L}| = 0.3$; hence, $\epsilon_0 \gg |U_{G_L}|$. The frequency-dependent imaginary (k) part of the refractive index of the dye-sensitized nc-TiO_2 used in the calculations was

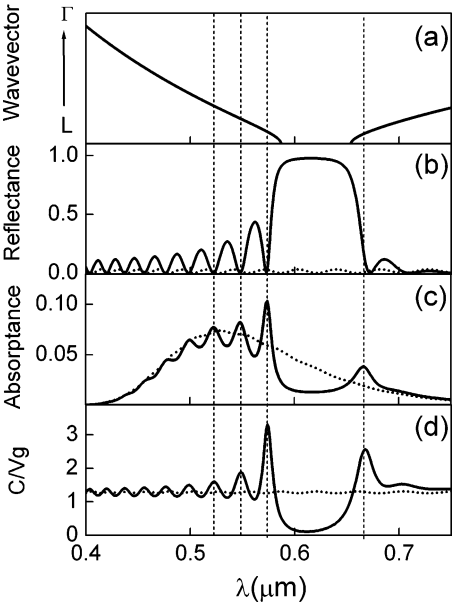

Figure 2. (a) Band structure along the Γ−L direction for a close-packed fcc structure made of spherical cavities with refractive index $n = 1.433$ and diameter $\phi = 220$ nm in a background of $n = 2.25$ (inverse nc-TiO_2 opal soaked in Solaronix Iodolyte TG50, as in ref 19). (b) Reflectance, (c) absorptance, and (d) ratio between light speed in a vacuum and group velocity (v_g) for a slab of a photonic crystal of the above-mentioned characteristics are shown as solid lines. Crystal thickness is 17 sphere monolayers (MLs), and the refractive indexes of the incoming and outgoing media are $n = 1.45$ (glass electrode) and $n = 1.433$ (the iodide solution), respectively. For the sake of comparison, reflectance, absorptance, and c/v_g of a standard DSSC having the same overall thickness and amount of absorbing material as the inverse opal slab are also shown in each case as dotted lines.

$$k(\lambda) = k_0\, e^{1 - z(\lambda) - e^{-z(\lambda)}} \quad z(\lambda) = \frac{\lambda - \lambda_0}{\Delta\lambda} \tag{20}$$

which was the result of fitting photocurrent and absorptance data reported for similar thin layers in the literature. In our case, $k_0 = 0.003$, $\lambda_0 = 538$ nm, and $\Delta\lambda = 64.16$ nm.

The optical reflectance and absorptance of the dye-sensitized oxide film when shaped in the form of an inverse opal are shown in Figures 2b and 2c, respectively (solid lines). For comparison, R and A of a thin layer of nonstructured dye-sensitized nc-TiO_2, as in the scheme in Figure 1a, are also plotted (dotted lines). To keep the same overall thickness and amount of absorbing material as in the photonic-crystal-based DSSC of Figure 1c, we assume that the cell used as a standard is made of an

absorbing dye-sensitized nc-TiO_2 slab having a pore volume and a thickness similar to that of the opal film with which it is to be compared.

In Figure 2b, a reflection peak is observed for photon wavelengths for which there are no allowed modes in the crystal in Figure 2a. The reflectance maximum at these stop-band frequencies does not reach unity and is wider than the gap predicted by the band calculation in Figure 2a. Both effects are consequences of the finite size of the crystal, which permits coupling of the evanescent stop-band waves to the outgoing medium. The side lobes also stem from the finite size of the crystal. In Figure 2c, it can be seen that a sharp increase of absorptance occurs in several narrow spectral ranges ($\Delta\lambda/\lambda \approx 1-2\%$) at both sides of the stop band as well as a wide deep decrease coincident with the stop-band position. The effective group velocity for photons crossing DSSCs like those shown in Figures 1a (dotted line) and 1c (solid line) is plotted in Figure 2d.

Comparison between all four plots in Figure 2 provides some hints on the origin of the observed changes in the optical losses. Vertical dashed lines are drawn to highlight the position of the absorptance maxima in Figure 2c. From this comparative analysis, we conclude that the absorption amplification seems to be the result of two types of slow photon propagation. First, for frequencies at the red edge of the stop band, the absorptance maximum position coincides with a maximum of the c/v_g curve in Figure 2d, that is, a group velocity minimum. At this edge, photons travel preferentially through the high dielectric constant path[22] (i.e., the dye-sensitized nc-TiO_2 walls of the inverse opal), and their speed is largely reduced as a consequence of the bending of the bands ($v_g = \partial\omega/\partial k$) at the *L*-point of the first Brillouin zone. A combination of the intrinsic finite absorption of the dye, light speed retardation, and percolation through the absorbing material results in a higher probability of absorption. This effect of slow photon propagation on optical absorption had already been observed at the gap edge of tungsten photonic crystals operating in the infrared, a sharp ($\Delta\lambda/\lambda < 4\%$) and intense absorptance peak being reported in that case.[42,43]

Second, within the higher-energy band, absorptance maxima positions match several reflectance minima at which group velocity is also smaller. These reflectance minima are the resonant modes of the photonic crystal film behaving as a Fabry−Perot cavity of homogeneous refractive index. Since the magnitude of the retardation is comparable for the band edge and some Fabry−Perot modes, so are the corresponding absorption amplification effects. Simulations were performed corresponding to illumination of the photonic crystal electrode from each one of the sides of the cell, which means that the incident medium is glass in one case and the electrolyte in the other, no significant differences being found.

From these results, it can be concluded that the overall effect of having just a periodically structured electrode would be the decrease in light-harvesting efficiency, since the enhancement observed at stop-band edges is less important than the depletion caused by the strong reflectivity at middle gap frequencies. So, the principle behind the almost 30% enhancement of photocurrent reported in ref 19 cannot be mainly the increased absorption of light travelling through the photonic crystal thin film at frequencies corresponding to the red edge of the photonic stop band, as was originally proposed therein. Furthermore, in the DSSC under analysis in that work, the stop band was centered at 610 nm, and the light-harvesting increase was measured over a wide wavelength range, namely, between 550 and 750 nm, which implies $\Delta\lambda/\lambda \approx 30\%$. (See Figure 3a, in which the photocurrent data reported in ref 19 are reproduced.) Thus, the optical absorption amplification was not only not restricted to the red edge of the gap, but it also swept the whole stop-band frequency range and extends down to the blue edge of the gap. Our calculations are in good qualitative agreement with recent experimental work reported in ref 26, in which a decrease in the conversion efficiency is observed for a photonic-crystal-shaped dye-sensitized nc-TiO_2 photoelectrode (not coupled to any other absorbing layer) with respect to that of a conventional DSSC.

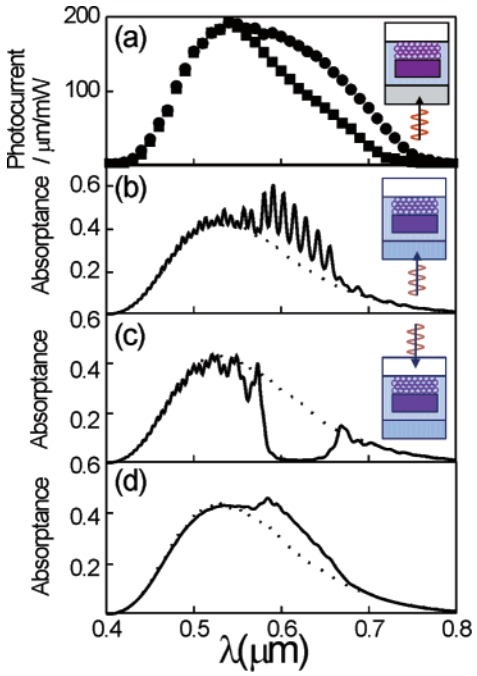

Figure 3. (a) Spectral variation of the photogenerated current, extracted from ref 19, corresponding to a bilayer DSSC like the one shown in the inset when illuminated from the rear side (circles) and to a nonperiodically structured, standard DSSC used for comparison (squares). Curves in parts b and c show the calculated absorptance (or LHE) for a structure similar to that reported in ref 19 under (b) rear and (c) front illumination. (d) Averaged absorptance of bilayer DSSCs formed by nc-TiO_2 inverse opals of different widths (from 3 to 17 sphere monolayers), each one of them having in turn different nc-TiO_2 layer thicknesses on top (from 6.5 to 7.5 μm). Rear side illumination was assumed. In parts b, c, and d, dotted lines are the calculated absorptance spectra of a standard DSSC having the same amount of absorbing material as in our bilayer system. The insets show schemes of the modeled structure, highlighting the corresponding illumination direction.

Absorptance of a Dye-Sensitized nc-TiO_2 Bilayer Structure (Inverse Opal + Dielectric Slab). A similar simulation was carried out for the photonic-crystal-based DSSC, taking into account the presence of a layer of dye-sensitized nc-TiO_2 on the photonic crystal photoelectrode (Figure 1c). This layer is usually spread by squeegee-printing of a commercially available nc-TiO_2 paste. In the case of ref 19, which we are taking as a model, it presented an average thickness of 7 μm. The porosity of such coatings is typically of 50%.[44] This empty volume is filled by the electrolyte, providing a large contact area between the dye-sensitized surface of the nanocrystals and the redox couple in solution.

The results for the absorptance calculations performed taking into account all these structural features are shown in Figures 3b and 3c (solid lines). Again, a comparison is made with an unstructured layer having a similar amount of absorbing material (dotted lines). In this case, to keep the same overall thickness and amount of absorbing material as in the photonic-crystal-based DSSC of Figure 1b, we assume that the cell used as a

standard is made of two absorbing dye-sensitized nc-TiO_2 slabs in a series, one having a pore volume and a thickness similar to that of the opal film with which it is to be compared and the other presenting a 50% porosity, as has been reported for conventional Grätzel photoelectrodes.

A clear asymmetric behavior with respect to the illumination direction was found. When light was assumed to reach the DSSC from the counter electrode side, a clear series of sharp, increased optical absorptance peaks extends throughout the whole stop-band frequency range, covering a wide spectral region (Figure 3b). Interestingly, LHE is enhanced mainly at stop-band frequencies. However, if light impinged from the conducting glass substrate side, then optical absorption decreased for all stop-band frequencies, which would result in an overall decrease in the photocurrent (Figure 3b).

These results are in good qualitative agreement with those reported in ref 19, from which, for the sake of comparison, we have extracted the photocurrent data plotted in Figure 3a. Both the wide spectral range at which optical absorptance amplification occurs and its strong dependence on the illumination direction arise in our model. However, the sharp peak structure of the curve in Figure 2b was not observed experimentally. To address these discrepancies, some other considerations were taken into account. First, squeegee-printing does not allow for precise control of the thickness of the deposited nc-TiO_2 layer over the whole cell surface. Therefore, the value of 7 μm reported in ref 19 may be considered just as an average thickness. Second, the fact that, even when vertical deposition allows for fine control of the colloidal crystal thickness over wide areas (17 sphere monolayers in our case), there will always be contributions to photocurrent coming from thinner regions at the edges when large areas of the cell are illuminated.

Therefore, to refine our calculation and better represent the real photonic-crystal-based DSSC, we also computed the absorption spectra for several photoelectrodes having photonic crystals of different thicknesses (from 3 to 17 sphere monolayers), each one of them having in turn different possible nc-TiO_2 layer thicknesses on top (from 6.5 to 7.5 μm). The whole set of spectra was then averaged, and the result is shown in Figure 3d. The effect of having different unstructured nc-TiO_2 layer thicknesses is mainly responsible for the wash out of the fine peak structure, while the presence of thinner colloidal crystals extends the optical absorption amplification toward higher wavelengths. When compared to Figure 3a, a fair agreement between our theory and the previously reported experiments is obtained.

An estimation of the increase in photocurrent generation efficiency can also be obtained by comparing the value of J_{SC} given by eq 1 for the bilayer DSSC with respect to that for the conventional DSSC used as a standard. Since $\Phi(\lambda)$ and $\xi(\lambda)$ are, in the range of interest, weakly dependent on λ, eq 1 becomes

$$J_{SC} \approx \int \mathrm{LHE}(\lambda)F(\lambda)\,\mathrm{d}\lambda = \int A(\lambda)F(\lambda)\,\mathrm{d}\lambda \qquad (21)$$

A standard solar spectral irradiance AM 1.5 spectrum divided by the photon energy was used as the photon flux in our calculations.[45] Applying eq 21 to the two absorptance spectra of Figure 3d and taking the ratio, we obtain a 21% enhancement of the photocurrent density in the bilayer DSSC with respect to that of the conventional DSSC used as a standard, in good agreemtent with the 26% reported in ref 19.

Origin of Absorption Amplification in the Bilayer Structure. As seen in the previous section, both the spectral response and the asymmetric behavior of the DSSC are fairly reproduced when the bilayer structure is considered. To analyze in more detail the origin of this absorption amplification effect at stop-band frequencies, both the effective group velocity and the spatial distribution of the square magnitude of the electric field were calculated for the bilayer structure when illuminated from the counter electrode side. Results are summarized in Figures 4 and 5. In Figure 4a, a closer look at the reflectance spectrum (solid line) calculated at stop-band frequencies shows that coupling to the bilayer is maximized (i.e., the reflectance is smaller) for certain narrow wavelength ranges. For these ranges, group velocity, plotted as a solid line in Figure 4b, is decreased with respect to the group velocity calculated for a conventional photolectrode layer in which no photonic crystal is present (dotted line). Wavelengths at which decreased and increased group velocity are observed are pointed out by vertical dotted lines in Figure 4, namely, λ_1 and λ_2, respectively. Furthermore, comparison between the spectral variation of the group velocity (Figure 4b) and the absorptance (Figure 4c) clearly indicates that optical losses are amplified at those wavelengths at which light travels more slowly through the bilayer, as happens for the case of the photonic crystal photoelectrode treated above, although now this enhancement sweeps the whole stop-band width instead of taking place just at the edges.

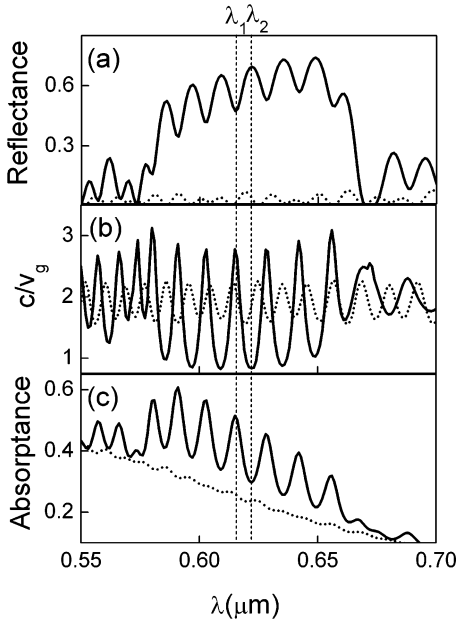

Figure 4. (a) Reflectance, (b) ratio between light speed in a vacuum and group velocity, and (c) absorptance of a 7-μm-thick dye-sensitized titania film deposited onto a 17 sphere monolayer inverse dye-sensitized titania photonic crystal immersed in electrolyte ($n = 1.433$) (solid lines). For the sake of comparison, (a) reflectance, (b) c/v_g, and (c) absorptance of a standard DSSC having both the same overall thickness and the amount of absorbing material as the bilayer are also shown (dotted lines). λ_1 and λ_2 are wavelengths at which a minimum and a maximum in the absorptance spectrum are observed.

Further insight into the question of *where* the absorption is actually occurring is provided by the analysis of the spatial distribution of the *absorbed* electric field intensity along the direction perpendicular to the cell substrate (*x*-axis), which is shown in Figure 5 (solid line). Its value has been estimated by subtracting the electric field propagating through the absorbing bilayer, $|\mathbf{E}|^2_{n+ik}$, from the electric field propagating through a similar bilayer but in which the imaginary part of the refractive index (i.e., the dye), responsible for the absorption, has been removed, $|\mathbf{E}|^2_n$. Field values are given by a set of equations (eq 12). Since $|\mathbf{E}|^2_n - |\mathbf{E}|^2_{n-ik}$ is proportional to the absorbed

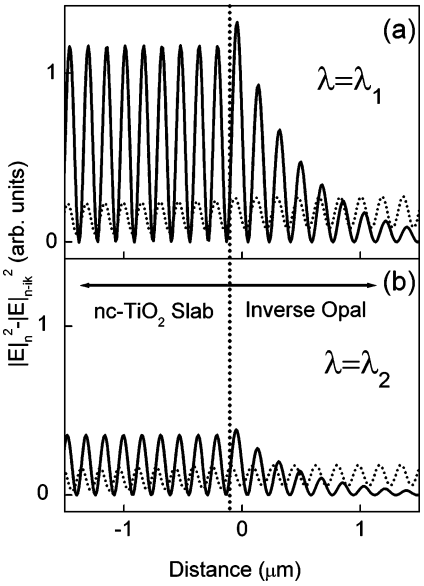

Figure 5. Estimation of the spatial distribution of the electric field intensity absorbed by the dye at two different wavelengths, namely, (a) $\lambda_1 = 0.615$ μm (a reflectance minimum) and (b) $\lambda_2 = 0.622$ μm (a reflectance maximum). A 7-μm-thick dye-sensitized titania film was deposited onto a 17 sphere monolayer inverse dye-sensitized titania photonic crystal immersed in electrolyte ($n = 1.433$) (solid lines.). For the sake of comparison, a spatial distribution of the square magnitude of the electric field absorbed by the dye in a standard DSSC is also shown (dotted line). The vertical dotted line represents the interface dye-sensitized nc-TiO_2 film and dye-sensitized inverse TiO_2 opal.

intensity in each part of the bilayer structure, its spatial distribution allows us to estimate in which part of the bilayer the absorption amplification is taking place. To know this, $|\mathbf{E}|^2_n - |\mathbf{E}|^2_{n-ik}$ versus x in the bilayer must be compared with $|\mathbf{E}|^2_n - |\mathbf{E}|^2_{n-ik}$ versus x along a conventional photoelectrode, in which no photonic crystal is present, having the same total thickness as the bilayer and the same total amount of dye. So, the same calculation is performed for such a system and shown in Figure 5 (dotted line).

When Figure 4b and Figure 5a are compared, the relation between slow group velocity and localization is made explicit. As expected, $|\mathbf{E}|^2_n - |\mathbf{E}|^2_{n-ik}$, corresponding to a mode at which the group velocity v_g is low (λ_1 in Figure 4a), is much larger than $|\mathbf{E}|^2_n - |\mathbf{E}|^2_{n-ik}$ in the conventional photoelectrode. However, interestingly, that happens *only* in the nanocrystalline coating part of the bilayer and in a thin region within the photonic crystal, very close to the interface. This means that most of the absorption amplification effect occurs in the nanocrystalline coating rather than in the photonic crystal. As we move away from the interface and deeper into the crystal, this amplification effect vanishes, neglected by the strong decay of the evanescent waves resulting from the presence of a stop band. However, modes at which the group velocity increases (such as λ_2 in Figure 4a) present a value of the absorbed intensity in that external slab much closer to that of the conventional photoelectrode and a similar behavior in the photonic crystal.

These results indicate that the observed absorptance peaks are a consequence of the appearance of resonant modes, localized preferentially at the absorbing nanocrystalline slab deposited onto the inverse opal. These modes are caused by the mirror behavior of the photonic crystal in the bilayer, a mirror that is porous both morphologically and optically. Waves coming from the counter electrode side and with frequencies within the stop-band range are evanescent and therefore penetrate the photonic crystal to a certain depth. An effective resonant cavity is then formed whose width is the thickness of the nanocrystalline coating plus a certain frequency-dependent penetration length in the crystal, above which the wave can be considered as totally attenuated. *It can be stated that coupling a photonic crystal to an absorbing nanocrystalline slab induces photon localization for certain frequency ranges within that slab, which implies slow propagation speed. This, in turn, yields a much higher probability of the photon being absorbed by the dye molecules in that slab.*

Optical properties of similar types of structures but made of transparent materials have recently been described, both experimentally and theoretically.[27] In that case, increased transmittance is detected for just one frequency range within the photonic gap of the crystal as a result of the presence of the thin (on the order of hundreds of nanometers) dielectric slab on its surface. The number of these surface resonant modes, their spectral position, and the intensity of the corresponding transmittance peaks (in the case of transparent materials) are mainly deter-

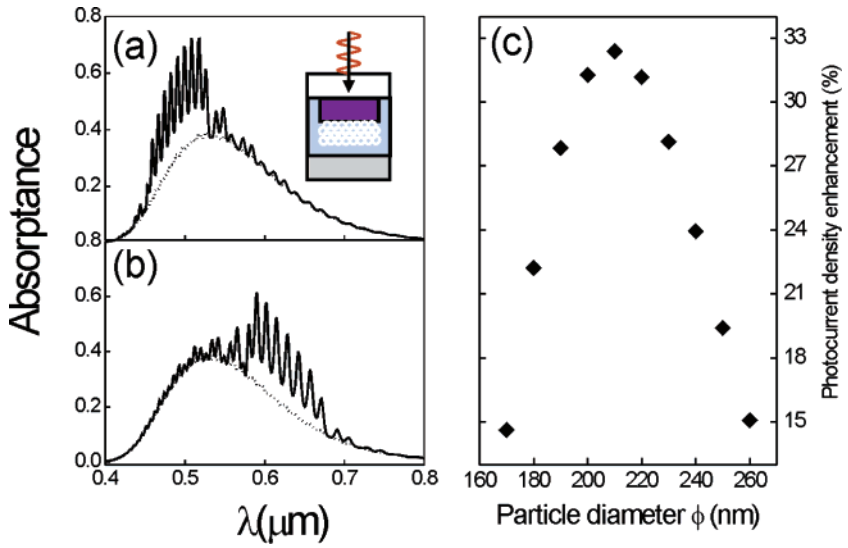

Figure 6. (a) Absorptance spectra of a 17 sphere monolayer inverse dye-sensitized titania photonic crystal of (a) $\phi = 180$ nm or (b) $\phi = 230$ nm deposited onto a 7-μm-thick dye-sensitized titania film that lays on a conductive glass substrate. The whole system is fully immersed in a medium of $n = 1.34$ (solid lines). For the sake of comparison, absorptance spectra of a standard DSSC is also shown (dotted line). (c) Photocurrent density enhancement (%) versus the diameter ϕ (nm) of the spheres of the photonic colloidal crystal.

mined by the thickness of the unstructured layer and the scattering strength of the photonic crystal. In the case that interests us here, the thickness of the surface slab is much larger than that in ref 27. For the typical thicknesses obtained by squeegee-printing (5−20 μm), the number of resonant modes is large, so the whole band-gap width is holed with sharp high transmittance windows at which photons will propagate slowly, as can be seen in Figures 4a and 4b.

Optimized and Alternative Photonic-Crystal-Based DSSC Designs. Our analysis indicates that the absorption amplification takes place for the resonant modes of a cavity formed by the inverse opal and the nanocrystalline coating when light impinges from that coating side. However, since our calculations indicate that the absorption amplification occurs mainly in the latter, we evaluated the possibility of keeping the same effect but using a colloidal crystal mirror in which no absorption takes place. Calculations confirmed this hypothesis. Absorptance spectra were calculated for a DSSC photoelectrode made of an inverse TiO_2 opal *on which no dye is adsorbed* deposited onto a conventional dye-sensitized nc-TiO_2 slab. A schematic of such a structure is depicted in Figure 1d. Results are shown in Figures 6a and 6b. Two different lattice parameters are considered to show the possibility of tailoring the amplification effects to measure along the absorption band of the dye. For these calculations, we assumed a refractive index of the liquid medium of $n = 1.34$, which would correspond to available acetonitrile-based electrolytes.

Figure 6c shows the photocurrent density enhancement versus the spherical cavity diameter for a cell like the one shown in the inset of Figure 6a. In practice, the cavity size is determined by the size of the original polystyrene bead used in the opal template. This enhancement of efficiency is the ratio between the J_{SC} obtained from eq 13 for the photonic-crystal-based DSSC and that calculated for a standard cell having the same amount of absorbing material, as defined in previous sections. Again, $F(\lambda)$ is assumed to be the standard AM 1.5 solar spectral irradiance divided by the photon energy. The spectra of the latter are shown in Figures 6a and 6b as dotted lines. From the plot in Figure 6c, it can be seen that the optimum performance of the bilayer structure is obtained when air cavities of diameters around 210 nm are built into the nc-TiO_2 inverse opal. This result reflects the importance of design when manufacturing a photonic-crystal-based DSSC, since a change in particle diameter of 20% can dramatically lower the efficiency enhancement by one-half.

Some other parameters can be modified to make a more efficient use of the solar spectrum. Larger absorptance peaks are observed when the scattering strength of the photonic crystal part of the cell is maximized. This strength depends basically on two parameters: dielectric contrast and filling fraction.[46] So, the larger the refractive index contrast between the electrolyte and the material of which the photonic crystal is made, the more intense the reflection at stop-band frequencies and therefore the higher the absorptance peaks due to localization in the absorbing coating. This happens for low values of the filling fraction of the high refractive index material.

In practical terms, the best choice for a colloidal structure is the one already reported in ref 19. Crystalline TiO_2 is the transparent material with the highest refractive index, and the inverse opal structure possesses a filling fraction close to the optimum values. However, from the viewpoint of materials processing, the fact that the colloidal crystal mirror does not need to absorb nor be conductor, as long as it is placed as in Figure 1d, opens the possibility of using different types of inverse opals or spherical colloids that could simplify the manufacturing process. Nowadays, spherical beads of numerous oxides and polymers can be attained both through direct synthesis[47] or by molding with inverse opals.[48] For instance, building up a colloidal crystal out of such microspheres would allow one to skip the calcinations process currently employed to build inverse titania opal photoelectrodes. So, the ease of fabrication might compensate for the lower performance due to increasing the filling fraction of the solid phase of the photonic crystal, which can be in turn compensated for by using lower refractive index electrolytes.

Conclusions

The origin of the enhancement of light-harvesting efficiency when a photonic crystal is introduced in a dye-sensitized nc-TiO_2-based solar cell has been studied. Comparison between the optical responses of different configurations led us to conclude that significant light absorption amplification over a wide spectral range occurs only in structures that combine the presence of a photonic crystal and a layer of nanocrystalline absorbing material. Our analysis indicates that the reported absorption enhancement occurs in resonant modes localized within the absorbing nanocrystalline coating rather than in the colloidal crystal, as has been previously been proposed. A deep insight into the optical response of such a structure is provided by the calculation of group velocity and the spatial distribution of the electric field. Experimental observations previously reported are successfully explained in these terms. Interestingly, our calculations show that there is no need to structure the light-harvesting material in the shape of a photonic crystal, efficient absorption being attained for a photovoltaic device in which a nonabsorbing, highly reflecting photonic crystal is implemented. Our results open the door to the use of a wide range of materials to build porous colloidal mirrors operating through coherent scattering.

Acknowledgment. This work has been funded by the Fundación Ramón Areces under the project "Colloidal Photovoltaic Materials".

References and Notes

(1) O'Regan B.; Grätzel, M. *Nature* **1991**, *353*, 737.
(2) Grätzel, M. *Nature* **2001**, *414*, 338.
(3) Bisquert, J.; Cahen, D.; Hodes, G.; Ruhle, S.; Zaban, A. *J. Phys. Chem. B* **2004**, *108*, 8106.
(4) Nazeeruddin, M. K.; Kay, A.; Rodicio, I.; Humphry-Baker, R.; Müller, E.; Liska, P.; Vlachopoulos, N.; Grätzel, M. *J. Am. Chem. Soc.* **1993**, *115*, 6382.
(5) Baruch, P. *J. Appl. Phys.* **1985**, *57*, 1347.
(6) Sayama, K.; Sugihara, H.; Arakawa, H. *Chem. Mater.* **1998**, *10*, 3825.
(7) Burnside, S.; Moser, J. E.; Brooks, K.; Grätzel, M. *J. Phys. Chem. B* **1999**, *103*, 9328.
(8) Tennakone, K.; Kumara, G. R. R. A.; Kottegoda, I. R. M.; Perera, V. P. S. *Chem. Commun.* **1999**, 15.
(9) Nazeeruddin, M. K.; Pechy, P.; Grätzel, M. *Chem. Commun.* **1997**, 1705.
(10) Wang, P.; Klein, C.; Humphry-Baker, R.; Zakeeruddin, S. M.; Grätzel, M. *J. Am. Chem. Soc.* **2005**, *127*, 808.
(11) Rothenberger G.; Comte, P.; Grätzel, M. *Sol. Energy Mater. Sol. Cells* **1999**, *58*, 321.
(12) Tachibana, Y.; Hara, K.; Sayama, K.; Arakawa, H. *Chem. Mater.* **2002**, *14*, 2527.
(13) Kay, A.; Grätzel, M. *Sol. Energy Mater. Sol. Cells* **1996**, *44*, 99.
(14) Usami, A. *Chem. Phys. Lett.* **1997**, *277*, 105.
(15) Kubo, W.; Sakamoto, A.; Kitamura, T.; Wada, Y.; Yanagida, S. *J. Photochem. Photobiol., A* **2004**, *164*, 33.
(16) Ferber, J.; Luther, J. *Sol. Energy Mater. Sol. Cells* **1998**, *54*, 265.

(17) Usami, A. *Sol. Energy Mater. Sol. Cells* **2000**, *64*, 73.
(18) Yablonovitch, E. *Phys. Rev. Lett.* **1987**, *58*, 2059.
(19) Nishimura, S.; Abrams, V.; Lewis, B. A.; Halaoui, L. I.; Mallouk, T. E.; Benkstein, K. D.; Lagemaat, J.; Frank, A. J. *J. Am. Chem. Soc.* **2003**, *125*, 6306.
(20) Huisman, C. L.; Schoonman, J.; Goossens, A. *Sol. Energy Mater. Sol. Cells* **2005**, *85*, 115.
(21) Kavan, L.; Zukalova, M. T.; Kalbac, M.; Grätzel, M. *J. Electrochem. Soc.* **2004**, *151*, A1301.
(22) Sakoda, K. *Optical Properties of Photonic Crystals*; Springer-Verlag: Berlin, Heidelberg, 2001.
(23) Vlasov, Yu. A.; Petit, S.; Klein, G.; Hönerlage, B.; Hirliman, Ch. *Phys. Rev. E* **1999**, *60*, 1030.
(24) Imhof, A.; Vos, W. L.; Sprik, R.; Lagendijk, A. *Phys. Rev. Lett.* **1999**, *83*, 2942.
(25) Light interferometry experiments have recently provided an estimation of the amplification factors and the frequency ranges at which such amplification effects could be expected for finite-size colloidal photonic crystals. See: von Freymann, G.; John, S.; Wong, S.; Kitaev, V.; Ozin, G. A. *Appl. Phys. Lett.* **2005**, *86*, 053108.
(26) Halaoui, L. I.; Abrams, N. M.; Mallouk, T. E. *J. Phys. Chem. B* **2005**, *109*, 6334.
(27) Mihi, A.; Míguez, H.; Rodríguez, I.; Rubio, S.; Meseguer, F. *Phys. Rev. B* **2005**, *71*, 125131.
(28) Wijnhoven, J. E. G. J.; Vos, W. L. *Science* **1998**, *281*, 802.
(29) Nishimura, S.; Shishido, A.; Abrams, N.; Mallouk, T. E. *Appl. Phys. Lett.* **2002**, *81*, 4532.
(30) Satpathy, S.; Zhang, Z.; Salehpour, M. R. *Phys. Rev. Lett.* **1990**, *64*, 1239.
(31) Shung, K. W. K.; Tsai, Y. C. *Phys. Rev. B* **1993**, *48*, 11265.
(32) Mittleman, D. M.; Bertone, J. F.; Jiang, P.; Hwang, K. S.; Colvin, V. L. *J. Chem. Phys.* **1999**, *111*, 345.
(33) For the case of spherical scatterers, the expression of U_G is given by the Rayleigh−Gans expression, which can be found in Bohren, C. F.; Huffman, D. R. *Absorption and Scattering of Light by Small Particles*; John Wiley and Sons: New York, 1983; p 162.
(34) Kittel, C. *Introduction to Solid-State Physics*, 7th ed.; John Wiley and Sons: New York, 1996; p 189.
(35) Tarhan, I. I.; Watson, G. H. *Phys. Rev. B* **1996**, *54*, 7593.
(36) Vlasov, Y. A.; Deutsch, M.; Norris, D. J. *Appl. Phys. Lett.* **2000**, *76*, 1627.
(37) Míguez, H.; Yang, S. M.; Ozin, G. A. *Langmuir* **2003**, *19*, 3479.
(38) Zhang, Z.; Satpathy, S. *Phys. Rev. Lett.* **1990**, *65*, 2650.
(39) Bendickson, J. M.; Dowling, J. P.; Scalora, M. *Phys. Rev. E* **1996**, *53*, 4107.
(40) Jiang, P.; Ostojic, G. N.; Narat, R.; Mittleman, D. M.; Colvin, V. L. *Adv. Mater.* **2001**, *13*, 389.
(41) Tetreault, N.; Mihi, A.; Míguez, H.; Rodríguez, I.; Ozin, G. A.; Meseguer, F.; Kitaev, V. *Adv. Mater.*, **2004**, *16*, 364.
(42) Fleming, J. G.; Lin, S. Y.; El-Kady, I.; Biswas, R.; Ho, K. M. *Nature* **2002**, *417*, 52.
(43) Lin, S. Y.; Fleming, J. G.; Li, Z. Y.; El-Kady, I.; Biswas, R.; Ho, K. M. *J. Opt. Soc. Am.B* **2003**, *20*, 1538.
(44) Grätzel, M. *Prog. Photovoltaics* **2000**, *8*, 171.
(45) Obtained from the Renewable Resource Data Center, http://rredc.nrel.gov.
(46) Sözuer, H. S.; Haus, J. W.; Inguva, R. *Phys. Rev. B.* **1992**, *45*, 13962.
(47) Jiang X. C., Herricks T., Xia Y. N. *Adv. Mater.* **2003**, *15*, 1205.
(48) Jiang, P.; Bertone, J. F.; Colvin, V. L. *Science* **2000**, *291*, 453.